CHEMISTRY OF MATERIALS

ARTICLE

pubs.acs.org/cm

Surface Loss in Ozone-Based Atomic Layer Deposition Processes

Harm C.M. Knoops,[†,‡,*] Jeffrey W. Elam,[§] Joseph A. Libera,[§] and Wilhelmus M.M. Kessels[‡]

[†]Materials innovation institute, M2i, P.O. Box 5008, 2600 GA Delft, The Netherlands

[‡]Eindhoven University of Technology, P.O. Box 513, 5600 MB Eindhoven, The Netherlands

[§]Energy Systems Division, Argonne National Laboratory, Argonne, Illinois 60439, United States

ABSTRACT: The recombinative surface loss of O_3 was investigated and its effects on the initial growth, film uniformity, and film conformality in atomic layer deposition (ALD) processes were illustrated. To determine O_3 recombination probabilities over a wide range, a method was developed using high aspect ratio capillaries at the inlet to a mass spectrometer. Using this method, we measured O_3 recombination probabilities ranging from $<10^{-6}$ to $>10^{-3}$ depending on the composition and temperature of the capillary surface. We utilized these measurements to understand dramatic variations in O_3 loss observed during the initial growth of O_3-based ALD Pt on Al_2O_3 and vice versa. Next, we studied the uniformity of O_3-based ALD using ZnO ALD as a model system. Changes in the spatial uniformity of the ALD ZnO films and the O_3 concentration in the reactor as a function of the O_3 exposure were explained by a transition from reaction- to recombination-limited growth. This explanation was validated using a simple plug-flow model. Finally, we estimated the maximum aspect ratios that can be coated for a given O_3 recombination probability in O_3-based ALD processes using reasonable cycle times.

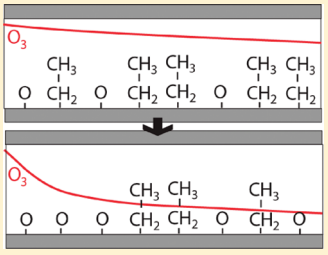

KEYWORDS: ALD, ozone, loss, recombination, decomposition

INTRODUCTION

Ozone (O_3) is being used in a growing number of atomic layer deposition (ALD) processes because O_3 is a powerful oxidizer and is easier to purge than H_2O, particularly at lower growth temperatures. Several ALD processes with excellent thickness uniformity and conformality have been demonstrated using O_3.[1−6] However, in some cases O_3 can thermally decompose on surfaces in recombination processes leading to poor thickness uniformity and conformality in the resulting ALD films.[6−9] This problem is particularly acute when the O_3 recombines rapidly on the material to be deposited. From heterogeneous catalysis it is known that the O_3 surface recombination rate depends greatly on both the chemical composition and the temperature of the surface.[10,11] With this in mind we can divide ALD materials into three groups: low loss oxides (e.g., SiO_2 and Al_2O_3), high loss oxides (e.g., MnO_2, Co_3O_4, NiO, Fe_2O_3, and CuO), and high loss noble metals and noble metal oxides (e.g., Pt and Rh_2O_3). The last group is special in that depending on conditions such as temperature and oxygen partial pressure, either the noble metal or the noble metal oxide is deposited. In previous studies of O_3-based ALD processes, severe thickness nonuniformities and the need for abnormally large O_3 exposures have been reported for the high-loss oxides Co_3O_4[7] and MnO_2[8] as well as the noble metal oxide Rh_2O_3.[9] With increasing growth temperature the rate of recombinative O_3 loss increases and this can have negative consequences for O_3-based ALD processes. For instance, a decrease in step coverage with increasing temperature was reported for the ALD of HfO_2 using O_3.[6]

For most ALD processes only surface losses for O_3 have to be considered, because losses from gas phase collisions between O_3 and other molecules are negligible at the typical pressures of 1−100 Torr.[12,13] The mechanism for O_3 surface loss on MnO_2 proposed by Li et al. is generally applicable to O_3 loss on other oxide surfaces.[14,15] Briefly, the mechanism consists of three steps as shown below. In step (i), an O_3 molecule reacts with a surface site (denoted with *) forming gaseous O_2 and an adsorbed O atom. In step (ii), another O_3 molecule reacts with the surface O forming gaseous O_2 and surface O_2. In step (iii) the surface O_2 desorbs as gaseous O_2 reopening up the surface site (*). The regeneration of the initial surface site shows that the O_3 surface loss process is catalytic. Step (i) is fast compared to steps (ii) and (iii) so that in steady state under O_3 exposure the surface is covered with surface O and O_2.

$$O_3(g) + * \rightarrow O_2(g) + O* \quad \text{(i)}$$

$$O_3(g) + O* \rightarrow O_2(g) + O_2* \quad \text{(ii)}$$

$$O_2* \rightarrow O_2(g) + * \quad \text{(iii)}$$

In atmospheric research, O_3 loss is typically quantified by a single loss probability per surface collision called the uptake coefficient.[16,17] Similarly, reactant loss in ALD can be quantified by a single loss probability per collision called the surface recombination probability.[18] The recombination probability can be used to predict the ability of an ALD process to conformally coat 3D structures as was shown in a recent simulation study for ALD using reactive gas phase species (e.g., plasma or O_3).[18] A high value for the surface recombination probability can greatly affect the conformality.[18] The surface recombination probability, *r*, should not be confused with the

Received: January 13, 2011
Revised: March 23, 2011
Published: April 14, 2011

reaction or sticking probability, s, which is the probability that an ALD precursor molecule will react upon colliding with the surface and contribute to film growth. The recombination probability depends strongly on the composition and temperature of the surface. For instance, addition of N_2 to the O_3 generator source gas is suggested to passivate the reactor surface by NO_2 or NO_3 species in HfO_2 ALD, thereby decreasing the O_3 recombination probability.[4] Also, the support material in the case of MnO_x particles can influence the O_3 recombination.[19]

To date, there have been no systematic studies of the effects of O_3 surface loss on ALD processes. The goal of this paper is to investigate recombinative O_3 loss under conditions relevant to ALD and illustrate its dependence on the temperature and the chemical composition of the surface, and its effects on film uniformity and conformality. We first describe a method using a high aspect ratio capillary installed at the inlet of a mass spectrometer to quantify O_3 recombination probabilities. Next, we use the mass spectrometer to monitor the changes in recombinative O_3 loss during ALD upon transitioning from a surface with low O_3 recombination to a surface with high O_3 recombination and vice versa. The influence of O_3 recombination on film uniformity was studied using O_3-based ZnO ALD as a model system. The changes in ZnO uniformity with increasing O_3 exposure time were simulated using a simple plug-flow model. Finally, the effects of O_3 recombination on conformality were estimated for a range of recombination probabilities.

EXPERIMENTAL SECTION

ALD Reactor. The ALD experiments used a viscous flow reactor,[20] constructed from a circular, stainless steel flow tube with a length of 1 m and an inside diameter of 5 cm to hold the substrates for film growth. A constant reactor temperature was maintained by four separate temperature controllers connected to resistive heating elements attached to the outside of the reactor. Ultrahigh purity (99.999%) nitrogen carrier gas continuously passed through the flow tube at a mass flow rate of 360 sccm and a pressure of 1 Torr. The following precursors were used: trimethyl aluminum ($AlMe_3$, Aldrich, 97%), bis(ethylcyclopentadienyl) manganese ($Mn(EtCp)_2$, Strem, 98%), trimethyl(methylcyclopentadienyl) platinum(IV) ($MeCpPtMe_3$, Aldrich, 98%), and diethyl zinc ($ZnEt_2$, Strem, 95%). The O_3 was produced using an O_3 generator (Ozone Engineering L11) using a feed of ultrahigh purity O_2 at a flow rate of 400 sccm to produce 5.5 volume percent O_3 in O_2 at an 80% level of maximum generator power. The generator was typically operated at a pressure of 810 Torr because this setting was found to reduce pressure transients during switching of the generator power. The ALD timing sequences will be expressed as t_1:t_2:t_3:t_4 where t_1 is the exposure time for the first precursor, t_2 is the purge time following the first exposure, t_3 is the exposure time for the reactant, and t_4 is the purge time following the exposure to the reactant. The pressure was monitored downstream of the flow tube by a 10 Torr Baratron capacitance manometer. The ALD reactor was equipped with a quadrupole mass spectrometer (QMS, Stanford Research Systems RGA300) located downstream of the flow tube in a differentially pumped chamber separated from the reactor tube by a 35 μm orifice and evacuated using a 50 l/s turbomolecular pump. For the surface recombination probability determination experiments, the orifice at the inlet of the QMS was replaced by a stainless steel capillary (45 mm length, 1.59 mm outer diameter, 127 μm inner diameter). Three capillaries were prepared. After first coating with 12 nm Al_2O_3 using 100 cycles of $AlMe_3/H_2O$ (5:10:5:10) at 200 °C, each capillary was coated with a different material using 30 cycles of ALD resulting in coatings of: 2.9 nm MnO_x, 3.4 nm Pt, and 5.4 nm ZnO. The ALD process conditions for the capillary coatings were: $Mn(EtCp)_2$ and H_2O (15:20:5:20) at 200 °C, $MeCpPtMe_3$ and O_2 (20:20:5:20) at 300 °C, and $ZnEt_2$ and H_2O (5:20:5:20) at 150 °C, respectively. Ellipsometric measurements of film thickness and refractive index were carried out for films deposited on Si(100) substrates using a J. A. Woollam alpha-SE spectroscopic ellipsometer (SE) system.

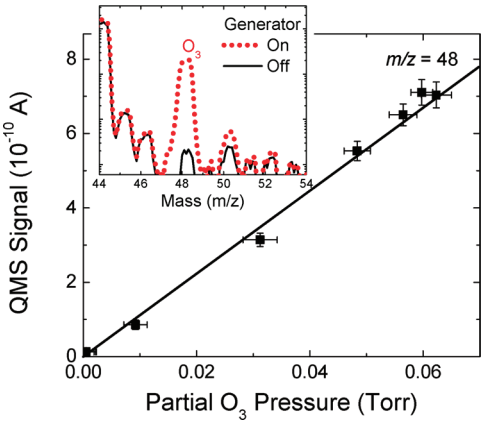

Figure 1. The QMS signal at m/z = 48 for a range of O_3 partial pressures. The inset shows the mass spectrum change when the O_3 generator is turned on.

Measurements of O_3 Concentration. Two methods were employed to measure the O_3 concentration in the ALD reactor. The first method used the pressure change upon switching on the O_3 generator and the second method was based on QMS. The pressure method is most suitable for steady state situations and gives directly the absolute O_3 partial pressure in the ALD reactor. The QMS method is typically better for qualitative measurements where relative changes in O_3 partial pressure need to be followed without disturbing the process.

The Baratron pressure gauge measures the absolute pressure and is independent of the gas species. When pure O_2 is flowing through the ALD system and the O_3 generator is switched on, a pressure decrease is observed on the pressure gauge as a portion of the O_2 is converted into O_3 according to the net reaction $3\ O_2 \rightarrow 2\ O_3$. Consequently, the converted portion of O_2 with partial pressure, p_{O2}, forms O_3 gas with partial pressure, $p_{O3} = {}^2/_3 p_{O2}$. The change in partial pressure measured by the pressure gauge is $\Delta p = {}^1/_3 p_{O2}$, which is half of the resulting partial pressure of the O_3, that is, $p_{O3} = 2\Delta p$.[21] This relationship assumes that the system pumping speed does not change and that the O_2 mass flow controller maintains a constant flow when the O_3 generator is turned on. According to the manufacturer, the pumping speed for the rotary vane mechanical pump is constant in the pressure regime used for these experiments. Furthermore, the assumption of constant O_2 flow was verified by monitoring the mass flow controller gain during the experiments.

Using the pressure method in an Al_2O_3 coated reactor at 100 °C, a concentration of 5 volume percent O_3 in O_2 was calculated which corresponds well with the manufactures' specification of 5.5 volume percent. Repeated measurements revealed that this method has a precision of ~10%. No measurable variation in O_3 concentration was found when the reactor temperature was changed from 100 to 300 °C suggesting little surface recombinative loss on Al_2O_3 within this temperature range. Therefore, an Al_2O_3 coated chamber was assumed to have negligible surface recombination of O_3 and was used as a standard reference.

When the O_3 generator was turned on, a clear signal was observed from the QMS at mass-to-charge ratio (m/z) = 48, indicative of O_3[16,22] as shown by the inset of Figure 1. The smaller QMS signal increase observed at m/z = 50 is consistent with an O_3 molecule where one oxygen atom is the naturally occurring isotope ^{18}O. The O_3 partial

dx.doi.org/10.1021/cm2001144 |Chem. Mater. 2011, 23, 2381–2387

Table I. Normalized Transmission Values, α, of O_3 for Various Capillary Coatings and Temperatures with AR = 350[a]

capillary	temperature	normalized transmission α	recombination probability *r*
Al_2O_3	100−200 °C	1	$<10^{-6}$
ZnO	100 °C	1	$<10^{-6}$
	150 °C	0.2 ± 0.1	$(5 \pm 2) \times 10^{-5}$
	200 °C	0	$>10^{-3}$
Pt	100 °C	0	$>10^{-3}$
MnO_x	100 °C	0	$>10^{-3}$

[a] The associated recombination probabilities were calculated using eq 1.

pressure was adjusted by controlling the O_3 generator power setting. Figure 1 shows the $m/z = 48$ signals for a variety of O_3 partial pressures as determined by the pressure method. The linear dependence between the $m/z = 48$ signal and the O_3 partial pressure demonstrates that the QMS can be used to accurately monitor the O_3 partial pressure. The advantage of the QMS method in monitoring O_3 during ALD processes as compared to the pressure method is the much higher selectivity for O_3 and weak sensitivity to background pressure fluctuations. Therefore, the QMS method does not require switching the generator power on and off under constant gas flow to determine the O_3 level. However, we found that the QMS had to be recalibrated frequently to ensure accurate measurements.

RESULTS AND DISCUSSION

O_3 Recombination. The O_3 recombination was first investigated in a qualitative way by measuring the O_3 reactor transmission for different reactor surface conditions. To explore the effects of the surface composition and surface temperature on the recombination process, the reactor walls were coated in situ with a series of ALD coatings and the reactor temperature was varied. Some surface conditions showed no steady state pressure differences and no $m/z = 48$ signals, indicating negligible O_3 transmission and a nearly complete recombination of O_3. These surfaces included NiO at 250 °C, Pt at 200−300 °C, and MnO_x at 200−300 °C. As mentioned previously, Al_2O_3 exhibited no change in the transmission probability for temperatures of 100−300 °C indicating negligible recombination in this temperature range.

The O_3 recombination probability, *r*, can be determined quantitatively by measuring the decrease in O_3 transmission through a capillary with a high aspect ratio. The large number of wall collisions that occur during transit through a high aspect ratio capillary greatly increase the probability for recombination and increase the sensitivity for low-loss processes. For these experiments, the orifice at the inlet of the QMS was replaced with a stainless steel capillary while the reactor chamber was precoated with Al_2O_3. To maintain a similar sensitivity of the QMS, the pressure difference between the reactor chamber and the QMS should be similar. Therefore, the gas conductance of the capillary and the orifice should be similar. The capillary has a larger diameter than the orifice (127 μm compared to 35 μm) to compensate for the decrease in conductance due to the higher aspect ratio (AR = 350 for the capillary compared to AR = ~3 for the orifice). With the Al_2O_3 coated capillary, the $m/z = 48$ signal was approximately the same as with the orifice indicating no decrease in O_3 transmission for Al_2O_3. Furthermore, increasing the temperature of the QMS inlet and capillary from 100 to

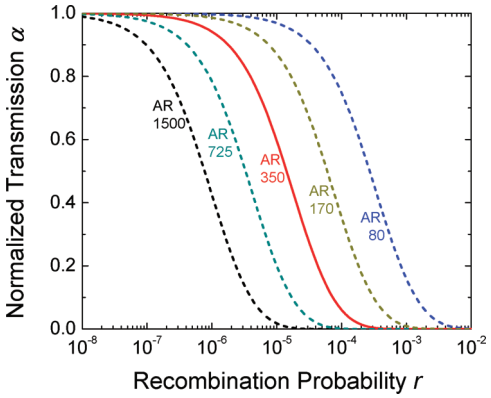

Figure 2. Normalized transmission, α, as a function of recombination probability, *r*, for capillaries with a range of aspect ratios (1500 − 80) according to eq 1.

200 °C showed no decrease in $m/z = 48$ signal. Therefore, the transmission for the Al_2O_3 coated capillary is not affected by O_3 surface recombination. For the coated capillaries, a normalized transmission, α, was defined as the $m/z = 48$ signal for the coated capillaries divided by the $m/z = 48$ signal measured after coating the capillary in situ with Al_2O_3 (the case with no O_3 surface recombination). The value α = 1 indicates that none of the particles reaching the end of the capillary have recombined, whereas α = 0 indicates complete recombination.

Table I summarizes the normalized transmission values measured using the capillary. Al_2O_3 (100−200 °C) and ZnO at 100 °C showed complete transmission of O_3 (α = 1). ZnO at 150 °C showed an incomplete but measurable transmission (α = 0.2), whereas ZnO at 200 °C and Pt and MnO_x at 100 °C showed no measurable O_3 transmission (α = 0).

Equation 1 relates the normalized transmission, α, the aspect ratio, AR, and the recombination probability, *r*, in the molecular flow regime:[18,23]

$$\alpha = \frac{1}{\cosh(\mathrm{AR}\sqrt{r})} \qquad (1)$$

Since the flow in the first part of the capillary was in the transition regime in our experiments (Knudsen number, $K = 0.9$ rather than $K \gg 1$ for molecular flow), there were still gas phase collisions and therefore the calculated *r* value will slightly underestimate the real *r* value. Equation 1 shows that for low AR and/or low *r*, α is close to 1, whereas for high AR and/or high *r*, α approaches zero. The *r* values calculated using eq 1 are shown in Table I. For Al_2O_3 and ZnO at 100 °C, $r < 10^{-6}$. For Al_2O_3 the value is similar to the value reported in the literature, $r = \sim 10^{-7}$.[13,17,24] For ZnO at 150 °C, $r = (5 \pm 2) \times 10^{-5}$, and for ZnO at 200 °C and Pt and MnO_x at 100 °C, $r > 10^{-3}$. The upper and lower bounds to the *r* values are estimated based on the uncertainty in our α measurements which are limited by the signal-to-noise ratio of the QMS measurements. The increase in *r* with temperature for ZnO agrees with the fact that O_3 recombination is a temperature activated process. The high values for MnO_x and Pt concur with the knowledge that MnO_x is an effective material for O_3 destruction and that Pt is reported to have even higher values of recombination than MnO_x.[25]

Figure 2 shows the normalized transmission, α, calculated using eq 1 for several aspect ratios in the range AR = 1500 − 80 including the aspect ratio for the capillary used in this work, AR = 350. For each

dx.doi.org/10.1021/cm2001144 |*Chem. Mater.* 2011, 23, 2381–2387

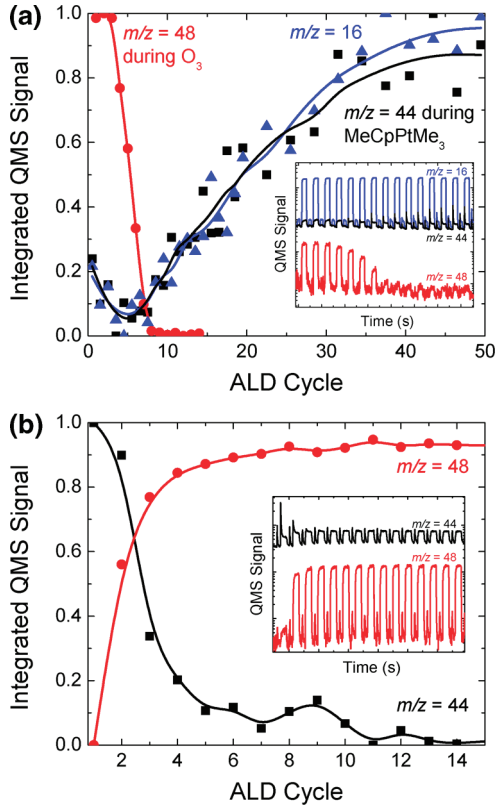

Figure 3. The integrated QMS signals for (a) $m/z = 16$ and $m/z = 44$ during the $MeCpPtMe_3$ exposures and $m/z = 48$ during the O_3 exposures for 50 cycles of Pt ALD on Al_2O_3 at 200 °C; and for (b) $m/z = 44$ and $m/z = 48$ during the O_3 exposure for 15 cycles of Al_2O_3 ALD on Pt at 200 °C. The integrated QMS signals were normalized to the range [0 - 1] and the insets shows the raw QMS data (for clarity only the first 15 cycles are shown for Pt ALD).

aspect ratio, a range of r values exists over which α is a sensitive function of r. For instance, at AR = 350, measurements of the normalized transmission coefficient allow exact determination of recombination probabilities in the range $\sim 10^{-6} - 10^{-4}$. For recombination probabilities outside of this range, the α measurements will only provide upper or lower bounds to r. For exact determination of lower or higher recombination probabilities, smaller or larger aspect ratios have to be employed. For instance, anodic aluminum oxide membranes could be used to obtain higher aspect ratios while maintaining sufficient gas conductance.[26] With the appropriate selection of high aspect ratio structures (e.g., AR = 1500, AR = 350, and AR = 80), this method can be used to determine the recombination probability over a range of several orders of magnitude and therefore also for a wide range of materials and temperatures.

Initial Stages of ALD Growth. To examine the effects of O_3 recombination on ALD nucleation and growth, we monitored the O_3 concentration and the gaseous reaction products during the ALD of a high r material (Pt) onto a low r material (Al_2O_3) by in situ QMS. For these experiments, 50 Pt ALD cycles were performed using $MeCpPtMe_3$ and O_3 with the timing sequence (5:5:10:5) on an Al_2O_3 coated chamber at 200 °C. Figure 3a shows the integrated QMS signals for $m/z = 16$ and $m/z = 44$ during the $MeCpPtMe_3$ exposures and the integrated QMS signals for $m/z = 48$ during the O_3 exposures. The integrated values were normalized and the inset shows the raw QMS data for the first 15 cycles.

We expect the mechanism for Pt ALD using $MeCpPtMe_3$ and O_3 to closely resemble Pt ALD using $MeCpPtMe_3$ and O_2 where combustion and ligand exchange reactions occur during the $MeCpPtMe_3$ exposures generating the reaction products CH_4, CO_2, and H_2O.[27,28] Consequently, $m/z = 16$ can be assigned to mainly CH_4 and cracking of $MeCpPtMe_3$ during the $MeCpPtMe_3$ exposure and mainly to cracking of O_2 and O_3 during the O_3 exposure. Furthermore cracking of CO_2 and H_2O can contribute to $m/z = 16$ during both steps. $m/z = 44$ can be ascribed to CO_2 during both steps, and $m/z = 48$ can be ascribed to O_3 during the O_3 exposure. Figure 3a shows that O_3 ($m/z = 48$) is stable for the first three cycles but then quickly decreases within a few cycles to a negligible level beyond 8 cycles. The reaction products CH_4 and CO_2 ($m/z = 16$ and $m/z = 44$) during the $MeCpPtMe_3$ exposures show an overall increase up to around 30 cycles suggesting a slow nucleation. This nucleation behavior corresponds to the late film closure observed in the literature at around 30−40 cycles.[29,30] Interestingly, the O_3 surface recombination starts already at the onset of the reaction products increase, suggesting a large influence of even a very small amount of Pt species on the O_3 transmission. Since Pt ALD can occur at 200 °C using O_2,[31] and most of the O_3 is lost due to recombination, most of the growth after the first few cycles probably occurs by reaction with O_2.

We next explored the effects of O_3 recombination on the ALD of a low r material (Al_2O_3) on top of a high r material (Pt). After first coating the ALD reactor with Pt, 15 cycles of Al_2O_3 ALD were performed using $AlMe_3$ and O_3 with the timing sequence (1:5:10:5) at 200 °C and the O_3 concentration and reaction products were monitored by in situ QMS. The gaseous reaction products during the O_3 exposures for Al_2O_3 ALD are mainly CH_4, with smaller amounts of C_2H_4, CO, and CO_2.[32,33] Figure 3b shows the normalized, integrated QMS signals for $m/z = 44$ (CO_2) and $m/z = 48$ (O_3) during the O_3 exposures and the inset shows the raw QMS data. The O_3 signal was initially negligible, but returned to a normal level after three cycles. Concurrently, a pressure drop was observed with the pressure gauge indicating an increase in the O_3 concentration (not shown). Although CO_2 is not a major product of the O_3 reaction for Al_2O_3 ALD on an Al_2O_3 surface, relatively large CO_2 signals were observed during the initial Al_2O_3 ALD cycles on the Pt surface (Figure 3b). On the same time scale as the O_3 QMS signals reappeared, the CO_2 QMS signals decreased to a negligible level. The initially higher CO_2 levels can be explained by the higher probability for ligand combustion in the presence of catalytic Pt or possibly by an initially higher probability of forming formate groups which decompose to produce CO_2.[32]

The initial growth of Pt on Al_2O_3 and vice versa showed dramatic changes in O_3 transmission in the first few ALD cycles, and these changes in O_3 concentration impacted the growth of the materials. Similar transients in O_3 concentration and concurrent changes in growth behavior have been observed during the ALD of In_2O_3 on Al_2O_3.[34] In general, such behaviors are expected for other combinations of materials with high and low r values. These pronounced changes reflect the strong effect that surface composition can have on the O_3 surface recombination probability.

Thickness Uniformity of ALD Films. O_3 recombination can lead to a progressive reduction in O_3 concentration along the flow direction in the ALD reactor and cause thickness nonuniformities. To investigate this phenomenon, the uniformity of ALD of ZnO using various reactants was compared. ZnO is

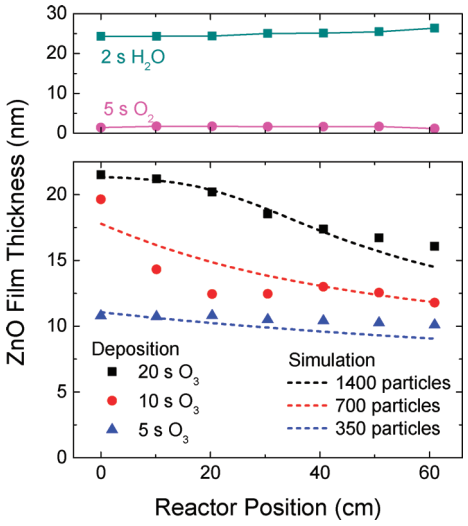

Figure 4. ZnO film thickness as a function of the position in the reactor where the $ZnEt_2$ and O_3 are introduced near 0 cm. The ZnO films were prepared using 150 cycles of $ZnEt_2$ (2 s) and either H_2O (2 s), or O_2 (5 s) (top graph), or O_3 (20, 10, or 5 s) (bottom graph). The dashed lines result from the plug-flow model simulation for 1400, 700, and 350 particles.

typically deposited using H_2O as reactant but ZnO has also been deposited using O_3 as reactant.[35] ZnO was deposited on an array of Si(100) samples evenly spaced along the flow direction of the ALD reactor over a distance of ~60 cm. After 150 cycles of ZnO ALD, the film thicknesses were measured using spectroscopic ellipsometry to generate a thickness profile. Thickness profiles were measured for a variety of different ZnO ALD conditions. These experiments used the timing sequence (2:10:*x*:10) where the O_3 exposure time, *x*, was 5, 10, and 20 s. For comparison, thickness profiles were generated in which the O_3 was replaced with H_2O (2 s exposures) and O_2 (5 s exposures). A deposition temperature of 200 °C was selected for these studies so that the O_3 recombination probability would be relatively high (Table I).

The top part of Figure 4 shows the thickness profiles measured using H_2O and O_2 as reactant. The thickness profile for H_2O is fairly uniform indicating saturating exposures for both $ZnEt_2$ and H_2O. As expected, virtually no ZnO was deposited using O_2 so that the O_2 contribution can be neglected for the profiles measured using O_3. The uniform profiles and the lack of growth using O_2 as reactant indicate that $ZnEt_2$ decomposition is not an issue at these conditions. The bottom part of Figure 4 shows the thickness profiles measured using O_3. At reactor position 0, the inlet of the reactor tube, the growth is roughly halfway saturated after 5 s O_3 and between 10 and 20 s O_3 the ZnO growth is nearly saturated. Interestingly, the thickness profile is quite uniform for the unsaturated growth at 5 s O_3, and is less uniform at 10 s. The thickness profile becomes more uniform again at 20 s when more regions in the reactor approach saturation. Furthermore, half of the growth occurs in the first 5 s of the exposure.

The $m/z = 48$ QMS signals recorded during the O_3 exposures for ALD ZnO thickness profile experiments are normalized to each other and shown in Figure 5. Initially, a high signal is seen which decreases with exposure time. The $m/z = 48$ signals for the 5, 10, and 20 s O_3 exposures overlap suggesting that the same surface is present at the beginning of the three different exposure times. The high initial signal indicates that at this point in the exposure, the O_3 loss due to reaction or recombination is low.

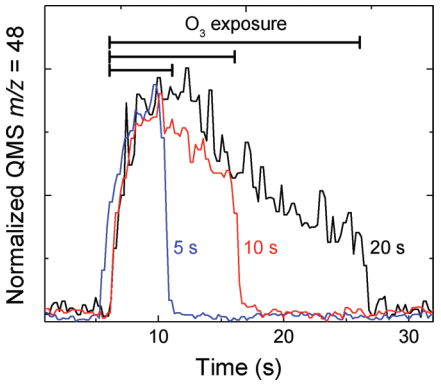

Figure 5. Normalized QMS $m/z = 48$ signals during the O_3 exposures of typical ALD ZnO cycles with O_3 exposure times of 5, 10, and 20 s. The O_3 exposure times are indicated by the horizontal black bars.

Similarly, the signal decrease with longer exposure times indicates greater O_3 loss due to reaction or recombination at the surface.

The ZnO film thickness profiles in Figure 4 can be analyzed by considering the evolution of surface species during each O_3 exposure. The expected surface reactions for ZnO ALD using $ZnEt_2$ and O_3 are shown below, based on the reaction mechanism of ZnO ALD using $ZnEt_2$ and H_2O,[36] and on the mechanism of Al_2O_3 ALD using $AlMe_3$ and O_3.[32] In these equations, "(ads)" represents an adsorbed species and "(g)" implies a gas phase species.

$$OH(ads) + ZnEt_2(g) \rightarrow OZnEt(ads) + EtH(g)$$

$$OZnEt(ads) + O_3(g) \rightarrow OZnOH(ads) + EtH(g) + CO_2(g) + H_2O(g)$$

Note that, this equation is unbalanced; knowledge of the ratio between reaction products would require additional quantitative measurements. By combining the results from Figure 4 and 5 several observations can be made. During the first 5 s of the O_3 exposures, the O_3 concentration remains relatively high and constant and the ZnO growth is uniform. These results imply that surface losses of O_3 due to both surface recombination and ligand elimination are small so that the ZnO ALD is reaction-limited during this period. After the first 5 s, the increase in thickness over most of the thickness profile is slow and the O_3 signal decreases indicating greater O_3 losses from surface recombination. This subsequent growth period (10 and 20 s O_3 exposure) resembles the recombination-limited regime described in our earlier work.[18] In the recombination-limited regime, surface recombination decreases the reactant concentration in the gas phase causing slow saturation over the entire substrate and poor thickness uniformity before reaching saturation. Apparently, the recombination probability on the initial ZnEt-terminated surface is much lower than on the ZnO or ZnOH surface. This explains why the initial ZnO growth is rapid and uniform and the O_3 concentrations are high. With this in mind, the evolution of the surface species and the O_3 concentration can be described as follows. Initially there is relatively little O_3 loss either by reaction or recombination on the ethyl covered surface resulting in a uniform, high O_3 concentration. As more ZnO or ZnOH surface is generated, more O_3 will be lost due to the faster recombination on these surfaces. At a certain ZnO

coverage, O_3 surface recombination will significantly deplete the O_3 concentration above the substrates leading to a concentration gradient and thinner ZnO films downstream in the reactor. Meanwhile, O_3 loss in the upstream part of the reactor will continue to increase due to the increasing ZnO surface coverage. Finally, the thickness gradient will gradually disappear and approach uniform saturation (as expected for ALD), but at a very slow rate due to the low O_3 concentration.

Plug-Flow Growth Model. The growth behavior described in the previous section has been simulated using a simple plug-flow model. The plug-flow approximation is reasonable since the system is in viscous flow,[20] and the flow rate in the axial direction (~2 m/s) is much higher than the axial diffusion rate (~0.02 m/s). Interestingly, at these pressures and flow rates the average number of collisions that a particle makes with the reactor tube walls is estimated from kinetic gas theory to be only ~25. This relatively low average number of collisions is due to the high number of gas phase collisions and the short residence time of 0.5 s in the 1 m long reactor tube. Reactions and losses due to gas phase collisions are neglected in this model. Briefly, the model consists of a 1D array of numbers, that is, cells, representing the reactor tube. Since each gas particle traversing the array interacts which each cell, each cell represents a wall collision. Since on average a particle makes 25 collisions, the array consists of 25 cells. At each cell the particle can react and stick with probability *s*, or it can recombine with probability *r*. A linear dependence for *s* and *r* on the ZnO coverage is assumed as typical in Langmuir adsorption. The ZnO coverage is defined as a local property for an area comprised of a group of Et ligands or ZnO units and is initially "0" when the area is fully covered with Et groups and becomes "1" when the saturation is complete, that is, when the surface is basically bare ZnO. The value of *s* decreases with the ZnO coverage, while the value of *r* increases with the ZnO coverage. The *r* values as determined in the first section would correspond with the end value of *r* at a ZnO coverage of "1".

For the case where *s* and *r* depend linearly on the ZnO coverage, reaction-limited, diffusion-limited, and recombination-limited growth,[18] can be simulated with this model. Furthermore, the general growth behavior observed in Figure 4 could be reproduced, that is, transitioning from reaction-limited to recombination-limited with a thickness profile change from uniform to nonuniform. However, for this simple linear dependence of *s* and *r* on the ZnO coverage, no good correspondence between the simulated and experimental profiles could be obtained. With the inclusion of a more physical representation of the dependence of *s* and *r* on ZnO coverage (multiple ZnO units needed for recombination, partial surface passivation at full coverage, and increased reactivity in the presence of recombination), reasonable agreement was obtained not only for profile shape but also for the dependence on exposure time. The dashed lines in Figure 4 show the uniformity profiles from the plug flow simulation for 1400, 700, and 350 particles. Note that, the exposures from experiment and simulation have the same ratios, that is, 4 to 2 to 1. Although passivation might appear counterintuitive compared to the high *r* value of ZnO at 200 °C, the *r* value after passivation is still higher than 10^{-3} which is the lower limit determined in the first section. Passivation was also reported in the literature and is suggested to involve peroxide species on the surface (O_2* in the decomposition mechanism in the introduction),[16] furthermore zinc peroxide (ZnO_2) is known to be stable up to 230 °C.[37]

Conformality of ALD Films. In principle, even for a material with a high O_3 recombination probability, good uniformity and conformality can be obtained by ALD when the reactant exposure is long enough. However, depending on the recombination probability, the saturating exposures for conformal deposition of a certain aspect ratio can be too long to be practical. Based on the recombination probabilities determined from the experiments in this study, the effect of O_3 recombination on the conformality that can be achieved by O_3-based ALD processes can be estimated. These estimates were made on the basis of a previous simulation study in combination with eq 1.[18] For materials with high *r* values, most aspect ratios would be in the recombination-limited regime and result in poor conformality before reaching saturation. The main question would be what aspect ratios can be coated practically, that is, using reasonable cycle times, for a given *r* value. As an order of magnitude estimate, aspect ratios at which the O_3 concentration decreases by a factor of 10 due to recombination ($\alpha = 0.1$ in eq 1) are taken as the maximum because higher aspect ratios would require unreasonably long O_3 exposure times. Table II shows the aspect ratios where $\alpha = 0.1$ for a range of *r* values. Conformal coating by ALD using O_3 of materials with these *r* values is estimated to be possible with reasonable cycle times for these aspect ratios. For Al_2O_3 (100−200 °C) and ZnO at 100 °C, AR values of 3000 or higher should be possible. For ZnO at 150 °C, the maximum AR value is around 400, and for ZnO at 200 °C and Pt and MnO_x at 100 °C, AR values of less than 100 will be practical.

Table II. Aspect Ratios for a Range of Recombination Probabilities *r* at which $\alpha = 0.1$ (eq 1)[a]

recombination probability *r*	aspect ratio at which $\alpha = 0.1$
0.1	10
0.01	30
0.001	100
10^{-4}	300
10^{-5}	1000
10^{-6}	3000

[a] Conformal coating of structures with these aspect ratios using O_3-based ALD is estimated to be possible with reasonable cycle times.

When saturating exposures for conformal and uniform deposition are too long to be practical, process conditions with a lower recombination probability are sought. Recombination can sometimes be decreased by using a reactant with negligible recombinative loss instead (e.g., H_2O or O_2). But in some cases there are no alternative reactants or the resulting films will lack the desired material properties. Another way to reduce surface recombination for O_3-based ALD processes is to lower the deposition temperature as we have demonstrated for ZnO. This method is likely to benefit a variety of ALD materials. However, in the case of In_2O_3 ALD using O_3,[34] it was found that the threshold temperature for ALD growth for the specific precursor employed coincided with the onset of O_3 thermal decomposition. So in this case lowering the growth temperature to boost conformality would not be possible. The possible passivation by peroxide species and the limited lifetime of the peroxide species,[15] suggests that in some cases a higher O_3 concentration and higher flux in terms of O_3 molecules per unit area and time can decrease the value of *r*. Addition of N_2 to the source gas of the O_3 generator can decrease the recombination probability in some cases but this N_2 addition might also influence the material properties and growth process.[4] For Fe_2O_3 and Pt it has been reported that the recombination probability decreases with increasing humidity.[17,38] Therefore, codosing O_3 and H_2O could offer

possibilities to improve uniformity and conformality for certain ALD processes.

CONCLUSIONS

A method using high aspect ratio capillaries as the inlet to the quadrupole mass spectrometer was developed to determine O_3 surface recombination probabilities over a wide range. The large differences in O_3 recombination probability between Pt and Al_2O_3 cause dramatic O_3 concentration changes upon transitioning between the ALD of these two materials, and these concentration changes are reflected in the growth mechanisms for the materials. These behaviors illustrate the profound effect that surface composition can have on O_3 recombination. The thickness uniformity of O_3-based ALD was studied using ZnO ALD as a model system. The evolution of the surface state and the O_3 concentration in the reactor was explained by a change in growth regime from reaction- to recombination-limited. Initially there is relatively little loss either by reaction or recombination on the ethyl covered surface. During growth the loss due to recombination increases because the ZnO coverage increases. This behavior could be simulated using a simple plug-flow model. The maximum aspect ratios are estimated for which conformal coating by ALD using O_3 can be achieved using reasonable cycle times. Overall, O_3 recombination depends greatly on the surface conditions and can have a large influence on film uniformity and conformality in ALD.

AUTHOR INFORMATION

Corresponding Author

*Phone: +31 40 247 2116. Fax: +31 40 245 6442. E-mail: H.C.M.Knoops@tue.nl.

ACKNOWLEDGMENT

This work was sponsored by the Materials innovation institute M2i (www.m2i.nl) under project number MC3.06278. The work at Argonne was supported by the U.S. Department of Energy, EERE-Solar Energy Technologies Program under FWP-4911A. Argonne National Laboratory is a U.S. Department of Energy Office of Science Laboratory operated under Contract No. DE-AC02-06CH11357 by UChicago Argonne, LLC.

REFERENCES

(1) Niinistö, L.; Ritala, M.; Leskelä, M. *Mater. Sci. Eng., B* **1996**, *41*, 23.
(2) Kim, J. B.; Kwon, D. R.; Chakrabarti, K.; Lee, C.; Oh, K. Y.; Lee, J. H. *J. Appl. Phys.* **2002**, *92*, 6739.
(3) Kim, J.; Chakrabarti, K.; Lee, J.; Oh, K. Y.; Lee, C. *Mater. Chem. Phys.* **2003**, *78*, 733.
(4) Delabie, A.; Caymax, M.; Gielis, S.; Maes, J. W.; Nyns, L.; Popovici, M.; Swerts, J.; Tielens, H.; Peeters, J.; Van Elshocht, S. *Electrochem. Solid-State Lett.* **2010**, *13*, 176.
(5) Rose, M.; Bartha, J. W.; Endler, I. *Appl. Surf. Sci.* **2010**, *256*, 3778.
(6) Liu, X. Y.; Ramanathan, S.; Longdergan, A.; Srivastava, A.; Lee, E.; Seidel, T. E.; Barton, J. T.; Pang, D.; Gordon, R. G. *J. Electrochem. Soc.* **2005**, *152*, G213.
(7) Klepper, K. B.; Nilsen, O.; Fjellvag, H. *Thin Solid Films* **2007**, *515*, 7772.
(8) Nilsen, O.; Fjellvσg, H.; Kjekshus, A. *Thin Solid Films* **2003**, *444*, 44.
(9) Hämäläinen, J.; Munnik, F.; Ritala, M.; Leskelä, M. *J. Electrochem. Soc.* **2009**, *156*, D418.
(10) Dhandapani, B.; Oyama, S. T. *Appl. Catal., B* **1997**, *11*, 129.
(11) Oyama, S. T. *Catal. Rev. - Sci. Eng.* **2000**, *42*, 279.
(12) Itoh, H.; Suzuki, T.; Suzuki, S.; Rusinov, I. M. *Ozone-Sci. Eng.* **2004**, *26*, 487.
(13) Itoh, H.; Rusinov, I. M.; Suzuki, S.; Suzuki, T. *Plasma Process. Polym.* **2005**, *2*, 227.
(14) Li, W.; Gibbs, G. V.; Oyama, S. T. *J. Am. Chem. Soc.* **1998**, *120*, 9041.
(15) Li, W.; Oyama, S. T. *J. Am. Chem. Soc.* **1998**, *120*, 9047.
(16) Hanisch, F.; Crowley, J. N. *Atmos. Chem. Phys.* **2003**, *3*, 119.
(17) Mogili, P. K.; Kleiber, P. D.; Young, M. A.; Grassian, V. H. *J. Phys. Chem. A* **2006**, *110*, 13799.
(18) Knoops, H. C. M.; Langereis, E.; van de Sanden, M. C. M.; Kessels, W. M. M. *J. Electrochem. Soc.* **2010**, *157*, G241.
(19) Radhakrishnan, R.; Oyama, S. T.; Chen, J. G. G.; Asakura, K. *J. Phys. Chem. B* **2001**, *105*, 4245.
(20) Elam, J. W.; Groner, M. D.; George, S. M. *Rev. Sci. Instrum.* **2002**, *73*, 2981.
(21) Daumont, D.; Brion, J.; Charbonnier, J.; Malicet, J. *J. Atmos. Chem.* **1992**, *15*, 145.
(22) Herron, J. T.; Schiff, H. I. *J. Chem. Phys.* **1956**, *24*, 1266.
(23) Walraven, J. T. M.; Silvera, I. F. *Rev. Sci. Instrum.* **1982**, *53*, 1167.
(24) Michel, A. E.; Usher, C. R.; Grassian, V. H. *Atmos. Environ.* **2003**, *37*, 3201.
(25) Chang, C. Y.; Tsai, W. T.; Cheng, L.; Chiu, C. Y.; Huang, W. H.; Yu, Y. H.; Liou, H. T.; Ku, Y.; Chen, J. N. *J. Environ. Sci. Health, Part A* **1997**, *32*, 1837.
(26) Feng, H.; Elam, J. W.; Libera, J. A.; Pellin, M. J.; Stair, P. C. *Chem. Eng. Sci.* **2009**, *64*, 560.
(27) Aaltonen, T.; Rahtu, A.; Ritala, M.; Leskelä, M. *Electrochem. Solid-State Lett.* **2003**, *6*, C130.
(28) Kessels, W. M. M.; Knoops, H. C. M.; Dielissen, S. A. F.; Mackus, A. J. M.; van de Sanden, M. C. M. *Appl. Phys. Lett.* **2009**, *95*, 013114.
(29) Christensen, S. T.; Elam, J. W.; Lee, B.; Feng, Z.; Bedzyk, M. J.; Hersam, M. C. *Chem. Mater.* **2009**, *21*, 516.
(30) Baker, L.; Cavanagh, A. S.; Seghete, D.; George, S. M.; Mackus, A. J. M.; Kessels, W. M. M.; Liu, Z. Y.; Wagner, F. T. *J. Appl. Phys.* **2011**.
(31) Aaltonen, T.; Ritala, M.; Tung, Y. L.; Chi, Y.; Arstila, K.; Meinander, K.; Leskelä, M. *J. Mater. Res.* **2004**, *19*, 3353.
(32) Goldstein, D. N.; McCormick, J. A.; George, S. M. *J. Phys. Chem. C* **2008**, *112*, 19530.
(33) Elliott, S. D.; Scarel, G.; Wiemer, C.; Fanciulli, M.; Pavia, G. *Chem. Mater.* **2006**, *18*, 3764.
(34) Elam, J. W.; Martinson, A. B. F.; Pellin, M. J.; Hupp, J. T. *Chem. Mater.* **2006**, *18*, 3571.
(35) Kim, S. K.; Hwang, C. S.; Park, S. H. K.; Yun, S. J. *Thin Solid Films* **2005**, *478*, 103.
(36) Ferguson, J. D.; Weimer, A. W.; George, S. M. *J. Vac. Sci. Technol. A* **2005**, *23*, 118.
(37) Chen, W.; Lu, Y. H.; Wang, M.; Kroner, L.; Paul, H.; Fecht, H. J.; Bednarcik, J.; Stahl, K.; Zhang, Z. L.; Wiedwald, U.; Kaiser, U.; Ziemann, P.; Kikegawa, T.; Wu, C. D.; Jiang, J. Z. *J. Phys. Chem. C* **2009**, *113*, 1320.
(38) Tsai, W. T.; Chang, C. Y.; Jung, F. H.; Chiu, C. Y.; Huang, W. H.; Yu, Y. H.; Liou, H. T.; Ku, Y.; Chen, J. N.; Mao, C. F. *J. Environ. Sci. Health, Part A* **1998**, *33*, 1705.